

Anti-Icing Superhydrophobic Coatings

Liangliang Cao,[†] Andrew K. Jones,[‡] Vinod K. Sikka,[‡] Jianzhong Wu,[§] and Di Gao^{*†}[†]Department of Chemical and Petroleum Engineering, University of Pittsburgh, Pittsburgh, Pennsylvania 15261,[‡]Ross Technology Corporation, Leola, Pennsylvania 17540, and [§]Department of Chemical and Environmental Engineering, University of California, Riverside, California 92521

Received August 4, 2009. Revised Manuscript Received September 26, 2009

We use nanoparticle–polymer composites to demonstrate the anti-icing capability of superhydrophobic surfaces and report direct experimental evidence that such surfaces are able to prevent ice formation upon impact of supercooled water both in laboratory conditions and in natural environments. We find that the anti-icing capability of these composites depends not only on their superhydrophobicity but also on the size of the particles exposed on the surface. The critical particle sizes that determine the superhydrophobicity and the anti-icing property are in two different length scales. The effect of particle size on ice formation is explained by using a classical heterogeneous nucleation theory. This result implies that the anti-icing property of a surface is not directly correlated with the superhydrophobicity, and thus, it is uncertain whether a superhydrophobic surface is anti-icing without detailed knowledge of the surface morphology. The result also opens up possibilities for rational design of anti-icing superhydrophobic surfaces by tuning surface textures in multiple length scales.

Introduction

Inspired by the self-cleaning properties of lotus leaves,^{1,2} researchers have recently made significant progress in fabrication of superhydrophobic surfaces,^{3–10} on which water droplets bead up with a contact angle greater than 150° and drip off rapidly when the surface is slightly inclined. The superhydrophobicity, characterized by the high contact angle and small hysteresis of water droplets, on such surfaces has been attributed to a layer of air pockets formed between water and a rough substrate.^{11–13} One attractive application of superhydrophobic surfaces, in addition to the extraordinary water-repellency, is their speculated capability to reduce accumulation of snow and ice and to even completely prevent formation of ice on solid surfaces.^{14–16} Several groups have studied the adhesion of ice on superhydrophobic surfaces and have found correlations, with a reasonable degree of success, between reduction in ice adhesion and the superhydrophobicity of surfaces.^{14–16} However, we are unaware of published research to study ice formation on superhydrophobic surfaces.

Among numerous problems caused by icing, many are due to striking of supercooled water droplets onto a solid surface. Such

icing caused by supercooled water, also known as “freezing rain”, “atmospheric icing”, or “impact ice”, is notorious for glazing roadways, breaking tree limbs and power lines, and stalling airfoil of aircrafts, which may cause immeasurable economic losses.^{17,18}

Whereas extensive work has been published on superhydrophobicity, up to date there is little experimental/theoretical work on ice formation from supercooled water on superhydrophobic surfaces. The speculation on the anti-icing property of superhydrophobic surfaces, especially when supercooled water droplets strike such surfaces, has been under debate for many years.

In this work, we study the anti-icing property of superhydrophobic coatings prepared by using nanoparticle–polymer composites. We demonstrate that when the size of the particles in these composites is in the right range, the coatings are able to prevent ice formation upon impact of supercooled water both in laboratory conditions and in naturally occurring environments. More importantly, we find that the anti-icing capability of these composites depends not only on their superhydrophobicity but also on the size of the particles exposed on the surface. The critical particle sizes that determine the superhydrophobicity and the anti-icing property are in two different length scales. These results open up possibilities for rational design of anti-icing superhydrophobic surfaces by tuning surface textures in multiple length scales.

Experimental Section

Synthesis of Acrylic Polymer Resin. In a typical process, the acrylic polymer was synthesized by free radical polymerization of styrene, butyl methacrylate, and glycidyl methacrylate in toluene using azodiisobutyronitrile (AIBN) as the initiator. All these chemicals were purchased from Sigma-Aldrich. In a three-necked round-bottomed flask equipped with a magnetic stirrer, a condenser, a funnel, and a thermometer, 3 g of styrene, 15 g of butyl methacrylate, 4 g of glycidyl methacrylate, and 100 mL of toluene were mixed. The mixture was stirred and heated to 85 °C. The heat

*Corresponding author. E-mail: gaod@engr.pitt.edu. Telephone: 412-624-8488. Fax: 412-624-9639.

- (1) Barthlott, W.; Neinhuis, C. *Planta* **1997**, *202*, 1–8.
- (2) Neinhuis, C.; Barthlott, W. *Ann. Bot.* **1997**, *79*, 667–667.
- (3) Blossley, R. *Nat. Mater.* **2003**, *2*, 301–306.
- (4) Erbil, H. Y.; Demirel, A. L.; Avci, Y.; Mert, O. *Science* **2003**, *299*, 1377–1380.
- (5) Onda, T.; Shibuichi, S.; Sotah, N.; Tsujii, K. *Langmuir* **1996**, *12*, 2125–2127.
- (6) Sun, T. L.; Feng, L.; Gao, X. F.; Jiang, L. *Acc. Chem. Res.* **2005**, *38*, 644–652.
- (7) Gao, L. C.; McCarthy, T. J. *J. Am. Chem. Soc.* **2006**, *128*, 9052–9053.
- (8) Tuteja, A.; Choi, W.; Ma, M. L.; Mabry, J. M.; Mazzella, S. A.; Rutledge, G. C.; McKinley, G. H.; Cohen, R. E. *Science* **2007**, *318*, 1618–1622.
- (9) Xiu, Y. H.; Zhu, L. B.; Hess, D. W.; Wong, C. P. *Nano Lett.* **2007**, *7*, 3388–3393.
- (10) Nakajima, A.; Hashimoto, K.; Watanabe, T. *Monatsh. Chem.* **2001**, *32*, 31–41.
- (11) Cassie, A. B. D.; Baxter, S. *Trans. Faraday Soc.* **1944**, *40*, 546–551.
- (12) Herminghaus, S. *Europhys. Lett.* **2000**, *52*, 165–170.
- (13) Lafuma, A.; Quéré, D. *Nat. Mater.* **2003**, *2*, 457–460.
- (14) Saito, H.; Takai, K.; Yamauchi, G. *Surf. Coat. Int.* **1997**, *80*, 168–171.
- (15) Nakajima, A.; Hashimoto, K.; Watanabe, T. *Monatsh. Chem.* **2001**, *132*, 31–41.
- (16) Kulinich, S. A.; Farzaneh, M. *Appl. Surf. Sci.* **2009**, *255*, 8153–8157.

(17) Cober, S. G.; Isaac, G. A.; Strapp, J. W. *J. Appl. Meteorol.* **2001**, *40*, 1984–2002.

(18) Lasher-Trapp, S.; Anderson-Bereznicki, S.; Shackelford, A.; Twohy, C. H.; Hudson, J. G. *J. Clim. Appl. Meteorol.* **2008**, *47*, 2659–2678.

source was then turned off. A solution of 0.2 g of AIBN in 2.5 mL of toluene was dropwise added into the flask. The reaction mixture was heated to 85 °C and stirred isothermally for 3 h. Afterward, the same amount of AIBN/toluene solution was added into the flask, and the mixture was stirred for another 3 h. At the end of the reaction, the mixture was cooled at room temperature. The resulting acrylic polymer was precipitated in hexane, filtered, and then dried under vacuum at 40 °C for 24 h. The molecular weight of the polymer was determined by gel permeation chromatography (Shimadzu). The number average molecular weight of the polymer was about 18 000 g/mol, and the weight average molecular weight was about 48 000 g/mol.

Preparation of the Polymer Binder. In a typical process, the polymer binder was prepared by mixing 2 g of the synthesized acrylic polymer, 1 g of silicone resin (DOW CORNING 840 RESIN, 60 wt % in toluene), 1 g of toluene, and 0.6 g of acetone. The binder can be cured either at room temperature for 12 h or at 80 °C for 2 h. During the curing process, the reactive glycidyl groups on the acrylic polymers cross-link with the silicone resin. The static water contact angle of the cured binder is $\sim 107^\circ$.

Preparation of the Particle–Polymer Composites. The particle–polymer composites were prepared by mixing about 2.5 g of the organosilane-modified silica particles of various diameters (20 nm, 50 nm, 100 nm, 1 μm , 10 μm , and 20 μm) with 5 g of the polymer binder, 75 g of toluene, and 15 g of acetone. They were applied on Al plates by using a spray gun at a pressure of about 30 psi and cured at room temperature for 12 h.

Electron Microscopy. Scanning electron microscopy (SEM) images and energy dispersive X-ray spectra were taken on a Philips XL-30 field emission SEM setup. A thin palladium/gold film was sputtered on the sample before SEM images were taken. Transmission electron microscopy images were taken using a JEOL 200CX microscope.

Contact Angle Measurement. The water contact angles were measured by using a VCA-OPTIMA drop shape analysis system (AST Products, Inc.) with a computer-controlled liquid dispensing system and a motorized tilting stage. Water droplets with a volume of 4 μL were used to measure the static water contact angle. The advancing and receding angles were recorded during expansion and contraction of the droplets induced by placing a needle in the water droplets and continuously supplying and withdrawing water through the needle. The sliding angle was measured by tilting the stage and recorded when the droplet began to move in the downhill direction. Each measurement was repeated three times. The measurement was performed under normal laboratory ambient conditions (20 °C and 30% relative humidity). The intrinsic water contact angle on the silica particles was estimated by measuring the water contact angle on a flat silica surface modified with the same surface chemistry.

Icing Experiments Using Laboratory-made Supercooled Water. Supercooled water was prepared by storing bottled pure water in a -20°C freezer for 3 h. The coated and uncoated Al plates were also stored in the -20°C freezer for 3 h before the experiments and were tilted at an angle of about 10° to the horizontal plane during the experiments. A volume of 500 mL of supercooled water was poured onto the Al plates in about 10 s at approximately constant rate from a bottle located about 5 cm above. Occurrence of icing was determined by eye inspection. The experiment was repeated 20 times on each sample prepared with particles of a certain size. The icing probability for each sample was determined by dividing the number of experiments when icing occurred by the total number of experiments (20 in this case).

Icing Experiments Using Naturally Occurring Freezing Rain. One side of an Al plate (10 cm \times 10 cm) was coated with a superhydrophobic composite made with ~ 50 nm organosilane-modified silica particles, while the other side was untreated. A hole of about 1 cm in diameter was drilled near one edge of the plate and a cotton thread was used to hang the Al plate outdoors. Half of a commercial satellite dish antenna (SuperDish Network) was

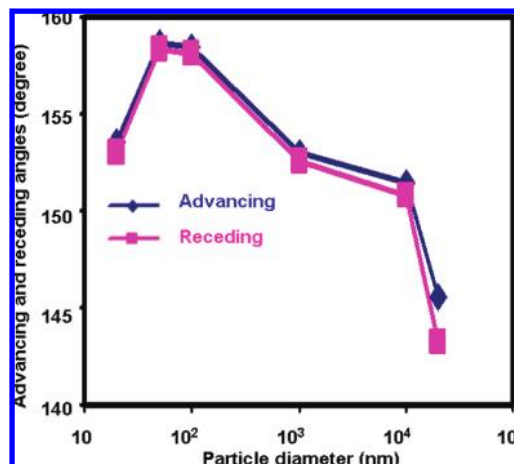


Figure 1. Advancing and receding water contact angles of particle–polymer composites as a function of the particle size.

coated with the same composite while the other half was untreated. Both the dish antenna and the Al plate were placed outdoors in typical weather conditions ($\sim -10^\circ\text{C}$) of Pittsburgh, PA, in January for 7 days before the freezing rain occurred on the night of January 27, 2009.

Results and Discussion

We made a series of particle–polymer composites by mixing a polymer binder with silica particles ranging from 20 nm to 20 μm in diameter. The polymer binder was synthesized by cross-linking a silicone resin with an acrylic polymer. The polymer binds strongly to many substrates, including metal and glass, and has an intrinsic water contact angle of $\sim 107^\circ$. The surface of the silica particles was modified with organosilane molecules. The intrinsic water contact angle of the surface-modified silica particles is $\sim 110^\circ$. The mixtures were sprayed onto Al plates and cured at room temperature for 12 h. Energy dispersive X-ray spectra of the polymer binder and the finished coating composed of polymer–particle composites are presented in Figure S1 in the Supporting Information. The spectrum shows that the prepared superhydrophobic coatings are fluorine-free.

The measured water contact angles of these composites are plotted in Figure 1. All the cured composites exhibit high water repellency. The composites prepared by using particles of 20 nm, 50 nm, 100 nm, 1 μm , and 10 μm in diameter all possess similar superhydrophobicity, characterized by the larger than 150° advancing and receding angles with less than 2° hysteresis. Only the composite prepared by using 20 μm particles has a less than 150° water contact angle and about 4° hysteresis.

To test the anti-icing capability of these composites, we poured supercooled water ($T = -20^\circ\text{C}$) onto the coated Al plates from ~ 5 cm above and visually inspected whether ice was formed upon impact. Figure 2 shows typical images taken during the experiment to demonstrate the anti-icing property of the superhydrophobic nanoparticle–polymer composites. Supercooled water (-20°C) was poured onto two Al plates; the right plate was untreated, while the left one was coated with a nanoparticle–polymer composite (with 50 nm particles). On the right plate, ice formed instantly when the supercooled water impacted the plate. In contrast, on the left, ice did not form on the plate surface but built up from the bottom edge where the plate was in contact with an untreated Al tray. It is evident that the coating on the left Al plate is very effective to prevent icing of supercooled water upon striking the surface.

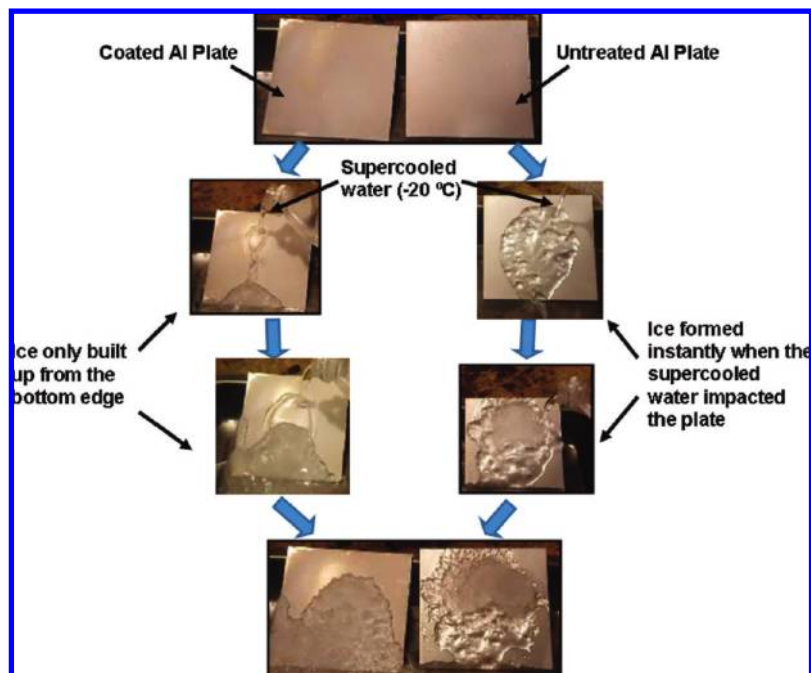


Figure 2. Optical images taken during the icing experiment that demonstrates the anti-icing property of a superhydrophobic nanoparticle–polymer composite. Supercooled water ($-20\text{ }^{\circ}\text{C}$) was poured onto two Al plates, one untreated (right) and one (left) coated with a nanoparticle–polymer composite (with particles 50 nm in diameter). The right plate was covered with ice instantly when it was in contact with the supercooled water. In contrast, ice did not form on the left plate when the supercooled water was poured on the surface; it built up from the bottom edge where the plate was in contact with an untreated Al tray.

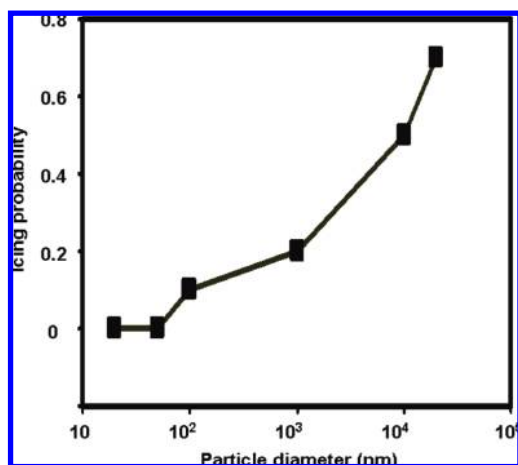


Figure 3. Icing probability as a function of the particle size.

We tested the anti-icing capabilities of other samples prepared with different particle sizes. The experiment was repeated 20 times on each sample to obtain the icing probability. Figure 3 shows the icing probability as a function of the particle size. A comparison of Figures 3 and 1 indicates that the critical particle sizes that determine the superhydrophobicity and the anti-icing property, respectively, are in two different length scales. Although composites made with particles up to $10\text{ }\mu\text{m}$ in diameter are all superhydrophobic, the anti-icing capabilities of these coatings are distinctly different: ice does not form on the samples prepared with 20 and 50 nm particles at all, but the icing probability increases remarkably when the particle diameter is larger than 50 nm.

Figure 4 shows three representative electron microscopy images of the cured composites with 20 nm, 50 nm, and $20\text{ }\mu\text{m}$ particles. Based on these images, the structure of the composites

and the profile of water in contact with the composites are schematically shown in Figure 5a. Water on these composites is primarily in contact with air pockets trapped in the rough surfaces. According to the Cassie–Baxter equation, the apparent contact angle (θ_{rough}) is related to the intrinsic contact angle (θ_{flat}) of a rough solid surface by¹¹

$$\cos \theta_{\text{rough}} = \phi_s \cos \theta_{\text{flat}} - (1 - \phi_s) \quad (1)$$

where ϕ_s is the area fraction of the solid in contact with the liquid. The large water contact angles on these composites imply that only less than 15% of the surface is in direct contact with water. Therefore, when supercooled water impacts such surfaces, icing may occur through a heterogeneous nucleation process at the contact between water and the particles exposed on the surfaces (Figure 5a). As a result, the kinetics of the ice nucleation process is determined by the size of the particles exposed on the surfaces.

The effect of the particle size on the free energy barrier of heterogeneous ice formation can be readily estimated by using a classical heterogeneous nucleation theory.¹⁹ In comparison with that for homogeneous nucleation (ΔG_c^{homo}), the free energy barrier for heterogeneous nucleation (ΔG_c) around a spherical particle of radius (R) is reduced by a factor (f) that varies from 1 to 0:

$$\Delta G_c = \Delta G_c^{\text{homo}} f \quad (2)$$

The effect of particle size on f can be calculated from:

$$f = \frac{1}{2} + \frac{1}{2} \left(\frac{1-mx}{w} \right)^3 + \frac{x^3}{2} \left[2 - 3 \left(\frac{x-m}{w} \right) + \left(\frac{x-m}{w} \right)^3 \right] + \frac{3mx^2}{2} \left(\frac{x-m}{w} - 1 \right) \quad (3)$$

(19) Liu, X. Y. *J. Chem. Phys.* **1999**, *111*, 1628–1635.

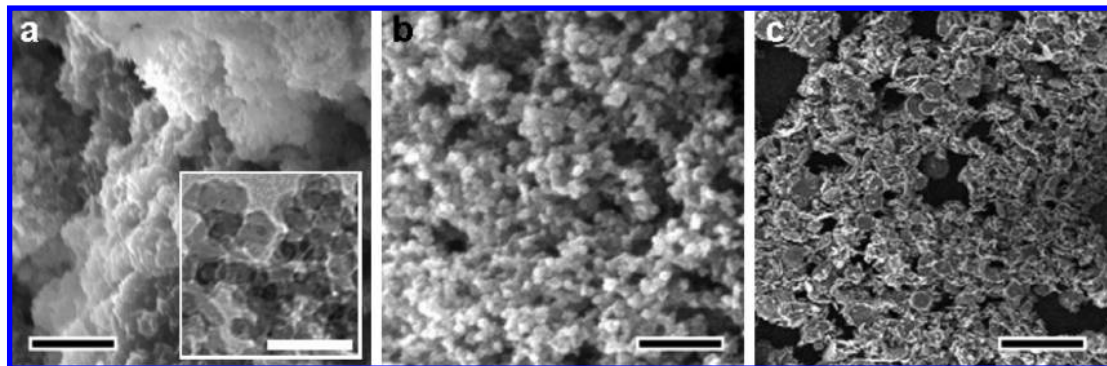


Figure 4. Representative electron microscopy images of the particle–polymer composites. (a) SEM image of a particle–polymer composite made of 20 nm silica particles. Scale bar = 1 μm . (Inset) Transmission electron microscopy image. Scale bar = 50 nm. (b) SEM image of a particle–polymer composite made of 50 nm silica particles. Scale bar = 1 μm . (c) SEM image of a particle–polymer composite made of 20 μm silica particles. Scale bar = 100 μm .

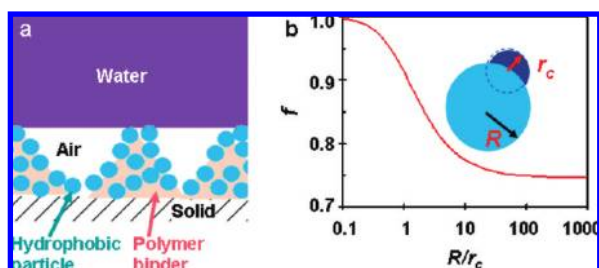


Figure 5. Heterogeneous nucleation on the surface of a superhydrophobic particle–polymer composite. (a) Schematic cross-sectional profile of water in contact with a superhydrophobic particle–nanoparticle composite. (b) Ratio (f) of the free-energy barrier for nucleation around a spherical particle relative to that in the bulk versus the relative particle radius (R/r_c).

where r_c is the radius of the critical nucleus, $x = R/r_c$, $m = \cos \theta_{\text{flat}}$ with $\theta_{\text{flat}} = 110^\circ$ for the hydrophobic silica particles, and $w = (1 + x^2 - 2xm)^{1/2}$. According to classical nucleation theory, the radius of the critical nucleus (r_c) can be estimated from

$$r_c = -\frac{2\gamma v}{\Delta G} \quad (4)$$

where $\gamma \approx 0.034 \text{ J m}^{-2}$ is the water–ice interfacial tension,²⁰ $v \approx 1.8 \times 10^{-5} \text{ m}^3 \text{ mol}^{-1}$ is the water molar volume, and $\Delta G \approx -C_p T [\ln(T/T_m) + T_m/T - 1]$. In this work, $T = 253.15 \text{ K}$ (-20°C), the ice melting temperature is $T_m = 273.15 \text{ K}$ (0°C), and the water heat capacity is $C_p \approx 75.3 \text{ J mol}^{-1} \text{ K}^{-1}$. r_c is calculated to be 21.6 nm under our experimental conditions.

Figure 5b presents the dependence of f on the relative particle radius (R/r_c) according to eq 3. It shows that f falls monotonically as R increases, which implies that the energy barrier (ΔG_c) continuously decreases as the particle size increases. Because the icing probability is an exponential function of the free energy barrier, the observed dramatic increase of the icing probability as the particle size increases can be readily explained.

We have also tested the anti-icing properties of the superhydrophobic composite in naturally occurring freezing rain. We coated one side of an Al plate with the composite made with 50 nm particles and left the other side untreated. The plate was left outdoors in winter for 1 week before freezing rain occurred. Figure 6a and b shows the two sides of the Al plate after the freezing rain: the side with the superhydrophobic composite has

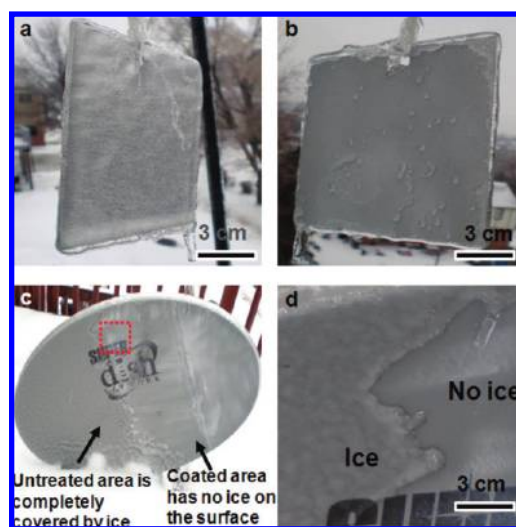


Figure 6. Test of anti-icing properties in naturally occurring “freezing rain”. (a) Untreated side of an aluminum plate after the natural occurrence of “freezing rain”. (b) Treated side of the aluminum plate coated with a superhydrophobic composite after the “freezing rain”. (c) Satellite dish antenna after the freezing rain. The left side is untreated and is completely covered by ice, while the right side is coated with the superhydrophobic composite and has no ice. (d) Close-up view of the area labeled by a red square in (c), showing the boundary between the coated (no ice) and uncoated area (ice) on the satellite dish antenna.

little ice, while the untreated side is completely covered by ice. Similar results were also obtained on a commercial satellite dish antenna (Figure 6c and d), where one-half of the dish was coated with the superhydrophobic composite and had no ice, but the other half was untreated and was completely covered by ice after the freezing rain. These results suggest significant application potential of the superhydrophobic nanoparticle–polymer composite as practical anti-icing coatings.

Conclusion

We have studied icing of supercooled water on superhydrophobic surfaces prepared using nanoparticle–polymer composites. We find that the anti-icing capability of these superhydrophobic surfaces is dependent strongly on the size of particles. This critical size, interestingly, is in a significantly different length scale compared to the critical size that determines the superhydrophobicity of these surfaces. This implies that caution

(20) Ketcham, W. M.; Hobbs, P. V. *Philos. Mag.* **1969**, *19*, 1161–1173.

needs to be taken when the anti-icing property is correlated to the superhydrophobicity, and it is uncertain whether a superhydrophobic surface is anti-icing without detailed knowledge of the surface morphology.

It is worth noting that the polymer binder synthesized and used in this work is not the only binder that may be used to make anti-icing superhydrophobic nanoparticle–polymer composites. We believe that many other polymer binders with a variety of compositions may also function in the same mechanism. Regardless of the composition of the coatings, it is important to recognize the two different length scales that determine the superhydrophobicity and the anti-icing property.

Icing of supercooled water on superhydrophobic surfaces is a complex phenomenon, and it may also depend on ice adhesion, hydrodynamic conditions, and structure of the water film on the surface. Further research is needed to understand the effect of these factors on icing. However, it is hoped that the experimental and theoretical results presented in this work may provide some

insights into this complex phenomenon and open up possibilities for rational design of anti-icing superhydrophobic surfaces by tuning surface textures in multiple length scales.

Acknowledgment. This work was supported by the National Science Foundation CMMI Grant #0626045 and the University of Pittsburgh Mascaro Sustainability Innovation Center. J.W. acknowledges the financial support by the U.S. Department of Energy (DE-FG02-06ER46296) and by the National Energy Research Scientific Computing Center (NERSC) under Contract No. DE-AC03-76SF0009.

Supporting Information Available: Representative energy dispersive X-ray spectra taken on (a) the synthesized polymer binders and (b) finished superhydrophobic coatings composed of polymer–nanoparticle composites. This material is available free of charge via the Internet at <http://pubs.acs.org>.